System Identification of Power Converters Based on a Black-Box Approach

Ju-Yeop Choi, *Member, IEEE*, Bo H. Cho, *Senior Member, IEEE*, Hugh F. VanLandingham, *Senior Member, IEEE*, Hyung-soo Mok, *Member, IEEE*, and Joong-Ho Song, *Member, IEEE*

***Abstract*— This paper addresses the topic of a model-free sys- tem identification of highly nonlinear power electronics systems from the data either through a time-domain simulation or a hardware measurement. Especially, this system identification method based on the black-box approach using the data generated from well-known design tools such as PSpice and MATLAB is generally simpler and independent of type of converters. As an application of identifying an unknown plant in power electronics systems, a constructive black-box approach is presented which aims at generating discrete-time small-signal linear equivalent models for a general class of converters, which includes resonant converters, pulsewidth modulation (PWM) converters and zero-voltage-switched (ZVS) PWM converters. The resulting small-signal model describes the converter as a linear time-invariant system, and the knowledge of the identified linear system can be applied to the switching converters for constructing feedback controllers. The identification results are compared with the analytical model and experimental data.**

I. Introduction

SWITCHING converters are inherently nonlinear oscillatory systems. A switching converter consists of linear resistors, inductors, capacitors, as well as nonlinear magnetic components and semiconductor switches. Especially, due to the severe nonlinear characteristics of magnetic components and switching devices, it is very difficult to design stable feedback controllers using exact mathematical descriptions of switching converters. Usually, switching converters have too many complex nonlinear differential equations to be solved.

Therefore, it is generally not feasible to construct design guidelines to regulate a converter in a large-signal domain. Instead, small-signal models are commonly used to provide dynamic information of the switching converters for control purposes, where the converter can be linearized around a specific operating point. Since the control issues of switching converters can be treated very effectively by small-signal analysis, the resulting small-signal models are very useful to design engineers on the grounds that all of the relatively simple techniques of linear system control theory can be applied easily to the small-signal model. Therefore, practicing engineers may acquire the physical insight of the given system for developing a proper feedback controller. From this small-signal model, important specifications such as audio susceptibility, loop gain, and output impedance are calculated. Additionally, these specifications can be easily measured whenever the small-signal model and/or the controller based on this model needs to be verified experimentally.

For the past decades, state-space averaging is a commonly used modeling approach for small-signal modeling of switching converters. This method was originally proposed to model pulsewidth modulation (PWM) converters. For properly designed PWM converters, the natural frequencies of each linear circuit are much lower than the switching frequency. This provides justification of the linear ripple assumption. Under the assumption that the natural frequency of the converter power stage is well below the switching frequency, the averaging technique can provide approximate linear solutions of a nonlinear averaged state equation. Then, the small-signal model can be derived by "persistently exciting" input signals around a particular operating point. The obtained small-signal model has a continuous form. The model can predict the dynamics of PWM-type converter power stages accurately up to the half of the switching frequency. The analysis of state-space averaging is simplified by using a circuit averaging technique based on three-terminal PWM switch model [1]. However, this averaging concept does not apply for resonant converters and multiresonant converters where the energy of state variables is carried mainly by switching harmonics but not by the low-frequency components as in the case of PWM-type converters. For resonant converters and multiresonant converters, the dynamics are often determined by the interaction between the switching frequency and the natural resonant frequency of the converter [2]. This interaction cannot be investigated using averaging concept because it eliminates the switching frequency information. In recent years, due to the specific circuit characteristics, the zero-voltage-switched (ZVS) PWM circuit topology has found many applications especially in high-voltage/high-power dc to dc converters. This ZVS PWM topology seems to be very close to the conventional PWM topology, but its small-signal properties are found to be significantly different from that of the PWM converter, and its small-signal analysis is hard to be achieved by state-space averaging because it would require solving the third-order system composed of six system equations whose averaging factors are implicit functions of the states [3].

Another systematic modeling method to obtain small-signal models for switching converters is a discrete-time (D-T) or a sampled-data modeling approach. By solving the nonlinear state equations in the time-domain, a steady-state analysis can

Manuscript received September 20, 1996; revised February 10, 1997, July 15, 1997. This paper was recommended by Associate Editor J. A. Nossek.

The authors are with the Bradley Department of Electrical Engineering, Virginia Polytechnic Institute and State University, Blacksburg, VA 24061-0111 USA.

Publisher Item Identifier S 1057-7122(98)07715-0.

be done under given operating conditions. Perturbation of this nonlinear equation around a specific operating point provides the small-signal dynamics with a sample interval the same as the switching frequency.

However, in recent years the area of modeling and analysis of power electronics systems, owing to their inherent nonlinear nature, has been a very difficult task in view of the lack of adequate analysis tools at the disposal of the circuit designer working in the field. Due to the increased speed, accuracy, and smaller size of today's high-performance regulators, new and more complex converter topologies have been continuously developed. It becomes an even more challenging task to develop a generalized modeling tool to analyze and design new circuit topologies.

In this paper, the topic of system identification of highly nonlinear power electronics systems from the data either through a time-domain simulation or a hardware measurement is presented. Especially, this system identification method based on the black-box approach using the data generated from well-known design tools such as PSpice and MATLAB is generally simpler and independent of type of converters. As an application of identifying an unknown plant in power electronics systems, a constructive black-box approach is presented which aims at generating discrete-time small-signal linear equivalent models for a general class of converters, which includes a PWM-type boost converter, a series-resonant converter, a multiresonant converter, and a ZVS PWM converter. Also, since this approach is a model-free identification, internal structure need not be known in advance as long as one can obtain a satisfactory statistical distribution of the data. This approach is also very effective to generate a reduced-order model to represent a complex subsystem in a distributed power system.

This paper is organized in the following way. The conventional method of multivariable system identification, which utilizes all possible observable structures of the system to achieve a linearized model, is presented briefly in Sections II-A and II-B. This method is used to optimally generalize over the available input/output data around an equilibrium point. Section III addresses the topic of the small-signal modeling of a highly nonlinear power electronics system, which is used to design feedback controllers. Finally, a discussion of the simulation results and some directions for the future work are presented in Section IV.

II. Multi-Input Multi-Output (MIMO) Structure Determination

A. System Identification

In his often referenced paper [4], Luenberger established nominal structures for a multi-input multi-output (MIMO) system. The method is based on the concept of either controllability or observability indexes. For present purposes only the observability form will be discussed. Beginning with an assumed D-T state-space model

$$\begin{aligned}\mathbf{x}(k+1) &= \mathbf{A}\mathbf{x}(k) + \mathbf{B}\mathbf{u}(k), \qquad \mathbf{x}(0)\\ \mathbf{y}(k) &= \mathbf{C}\mathbf{x}(k) + \mathbf{D}\mathbf{u}(k)\end{aligned} \tag{1}$$

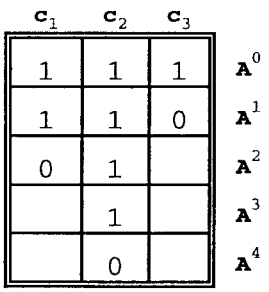

Fig. 1. Example of a crate diagram.

where $\mathbf{x}$ is an $(n \times 1)$ vector, $\mathbf{u}$ is an $(m \times 1)$ vector, $\mathbf{y}$ is a $(p \times 1)$ vector, and the matrices $\mathbf{A}$, $\mathbf{B}$, $\mathbf{C}$, and $\mathbf{D}$ have corresponding compatible dimensions, the observability matrix is given by the matrix $\mathbf{Q}_o$

$$\begin{aligned}\mathbf{Q}_o = \big[(\mathbf{c}_1)^T \cdots (\mathbf{c}_p)^T | (\mathbf{c}_1\mathbf{A})^T \cdots (\mathbf{c}_p\mathbf{A})^T |\\ \cdots | (\mathbf{c}_1\mathbf{A}^{n-1})^T \cdots (\mathbf{c}_p\mathbf{A}^{n-1})^T\big]^T.\end{aligned} \tag{2}$$

The dimensions of $\mathbf{Q}_o$ are $(np \times n)$. For an observable system $\mathbf{Q}_o$ must have rank n and, therefore, n linearly independent rows. The Luenberger form identifies the first n linearly independent rows from the top. The *observability index* for the pair $\{\mathbf{A}, \mathbf{C}\}$ is the smallest integer, ν, such that

$$\operatorname{rank}\big[\mathbf{C}^T \quad \mathbf{A}^T\mathbf{C}^T \quad \cdots \quad (\mathbf{A}^T)^{\nu-1}\mathbf{C}^T\big] = n. \tag{3}$$

Observability indexes (plural) are defined as the set of integers $\{\nu_i\}$, $1 \le i \le p$, identifying the lengths of the chains of each row of $\mathbf{C}$. For instance, the rows generated by row i are linearly independent up to (and including) $\mathbf{c}_i\mathbf{A}^{\nu_i-1}$. As an aid to the discussion, the crate diagram is introduced as a means of visualizing which n linearly independent rows of $\mathbf{Q}_o$ are being chosen [5]. As an example of a three-output system of order 7, consider Fig. 1. In this case the matrix of selected rows $\mathbf{T}$ becomes

$$\big[\mathbf{c}_1^T\mathbf{c}_2^T\mathbf{c}_3^T(\mathbf{c}_2\mathbf{A})^T(\mathbf{c}_2\mathbf{A})^T(\mathbf{c}_2\mathbf{A})^T(\mathbf{c}_2\mathbf{A}^2)^T(\mathbf{c}_2\mathbf{A}^3)^T\big]^T. \tag{4}$$

Note the correspondence between the partitions of $\mathbf{T}$ in (4) and the units in the crate diagram of Fig. 1. Using $\mathbf{T}$ as a similarity transformation matrix results in the equivalent state space model given by $\mathbf{A}_o = \mathbf{TAT}^{-1}$, $\mathbf{B}_o = \mathbf{TB}$, $\mathbf{C}_o = \mathbf{CT}^{-1}$, and $\mathbf{D}_o = \mathbf{D}$. This representation is in the *pseudo-observability form* (POF) state-space model corresponding to the indexes $\{2, 4, 1\}$, as indicated by the number of units in the three columns of the crate. The structure of the model is illustrated in the $\mathbf{A}_o$ and $\mathbf{C}_o$ matrices described below. The matrix $\mathbf{B}_o$ has no particular structure. The matrix $\mathbf{A}_o$ contains the remaining rows of the 7×7 identity matrix in rows 1, 2, 5, and 6. Its other rows may have arbitrary elements. The difference between a POF and the corresponding

Luenberger form is that Luenberger reordered the selected rows by the columns of the crate before performing the similarity transformation, a step which is not only unnecessary, but counterproductive in that the resulting structure is more complex!

$$\mathbf{A}_o = \begin{bmatrix} 0 & 0 & 0 & 1 & 0 & 0 & 0 \\ 0 & 0 & 0 & 0 & 1 & 0 & 0 \\ x & x & x & x & x & x & x \\ x & x & x & x & x & x & x \\ x & x & x & x & x & x & x \\ 0 & 0 & 0 & 0 & 0 & 1 & 0 \\ 0 & 0 & 0 & 0 & 0 & 0 & 1 \end{bmatrix}$$

$$\mathbf{C}_o = \begin{bmatrix} 1 & 0 & 0 & 0 & 0 & 0 & 0 \\ 0 & 1 & 0 & 0 & 0 & 0 & 0 \\ 0 & 0 & 1 & 0 & 0 & 0 & 0 \end{bmatrix}. \tag{5}$$

The idea behind the POF's is that the selection of the n linearly independent rows of $\mathbf{Q}_o$ can be done in many ways, according to the indices $\{n_1, n_2, \cdots, n_p\}$, representing the number of units in the p columns of the crate. The indexes must, of course, sum to n. Each possibility must be checked for "admissibility," i.e., that the resulting n rows are, in fact, linearly independent. The admissible POF's are then all possible structures for the MIMO system. Investigation of the various POF's for a particular system quickly indicates that some forms are better than others in terms of the condition number of the transformation matrix $\mathbf{T}$. A poorly conditioned transformation matrix typically results in a large range of parameter values in the POF, as well as loss of numerical accuracy in the model.

In Section II-B the deterministic identification algorithm is reviewed [6]. The identification technique presented in this paper, modified to accommodate noisy data, is given in Section III.

B. Deterministic Identification

In Section II-A the POF was introduced. The key is in the set of indexes specified for the POF in that everything related to the system structure is determined from them. In practice it is useful to establish an algorithm which will construct the POF given a basic state-space model and the information of the indexes. The reader is referred to [6] for details.

System identification from input/output data assumes that the input signals are "persistently exciting," i.e., that the system is sufficiently excited to exhibit all of its modes in the corresponding output signals. In addition, it is clear that only the controllable and observable part of the system can be identified from input/output data. To develop the necessary background, consider the desired result of the identification, namely, an order-n D-T system with m inputs and p outputs

$$\begin{aligned} \mathbf{x}(t+1) &= \mathbf{A}_o\mathbf{x}(t) + \mathbf{B}_o\mathbf{u}(t) \\ \mathbf{y}(t) &= \mathbf{C}_o\mathbf{x}(t) + \mathbf{D}_o\mathbf{u}(t) \end{aligned} \tag{6}$$

where $R_o = \{\mathbf{A}_o, \mathbf{B}_o, \mathbf{C}_o, \mathbf{D}_o\}$ is in a POF corresponding to a set of admissible POI, $\boldsymbol{\nu} = \{\nu_i\}$. From (6) we may write

$$\begin{bmatrix} \mathbf{y}(t) \\ \mathbf{y}(t+1) \\ \vdots \\ \mathbf{y}(t+r) \end{bmatrix} = \begin{bmatrix} \mathbf{C}_o \\ \mathbf{C}_o\mathbf{A}_o \\ \vdots \\ \mathbf{C}_o\mathbf{A}_o^r \end{bmatrix} \mathbf{x}(t) + \begin{bmatrix} \mathbf{D}_o & \cdots & 0 & 0 \\ \mathbf{C}_o\mathbf{B}_o & \cdots & 0 & 0 \\ & & \vdots & \\ \mathbf{C}_o\mathbf{A}_o^{r-1}\mathbf{B}_o & \cdots & \mathbf{C}_o\mathbf{B}_o & \mathbf{D}_o \end{bmatrix} \cdot \begin{bmatrix} \mathbf{u}(t) \\ \mathbf{u}(t+1) \\ \vdots \\ \mathbf{u}(t+r) \end{bmatrix}. \tag{7}$$

Now we let $r = \nu = \max\{\nu_i\}$. Clearly, (7) holds for any integer $t = [0, N-r]$ and can be rewritten as

$$\mathbf{y}_t = \mathbf{Q}_{oo}\mathbf{x}(t) + \mathbf{H}\mathbf{u}_t \tag{8}$$

where $\mathbf{y}_t$ and $\mathbf{u}_t$ are $(\nu+1)p$ and $(\nu+1)m$ dimensional columns containing output and input vectors $\mathbf{y}(t+j)$ and $\mathbf{u}(t+j)$, $j = [0, \nu]$. The matrix $\mathbf{Q}_{oo}$ is the observability matrix of the pair $\{\mathbf{A}_o, \mathbf{C}_o\}$, while $\mathbf{H}$ is the $(r+1)p \times (r+1)m$ lower block triangular matrix containing along the main diagonal the $(p \times m)$ blocks $\mathbf{D}_o$. The other nonzero blocks of $\mathbf{H}$ are the $(p \times m)$-dimensional *Markov parameters*

$$\mathbf{C}_o\mathbf{A}_o^j\mathbf{B}_o, \qquad \text{for } j = [0, \nu - 1]. \tag{9}$$

Our goal is to eliminate from (7) the $\mathbf{x}(t)$ terms, thereby obtaining an expression which relates the sampled data to the elements in R_o.

Equation (7) can be considered to represent $(\nu+1)p$ scalar equations in the samples

$$y_{ij} = y_i(t+j) \tag{10}$$

i.e., the ith component of the output vector $\mathbf{y}(t+j)$, $i = [1, p]$, $j = [0, \nu]$. It can be shown that $\mathbf{Q}_{oo}$ has n rows of an identity matrix and p rows that correspond to the rows of $\mathbf{A}_o$ with nonzero/nonunity elements. Furthermore, the locations of these rows are determined by the information of the indexes used to construct "selector matrices." The various selector vectors and matrices used in this development are all derivable from the set of indexes.

Premultiplying (8) by the selector matrices $\mathbf{S}_{li}^T$ and $\mathbf{S}_{ld}^T$ defined in [6], we obtain, respectively,

$$\mathbf{y}_{lt} = \mathbf{x}(t) + \mathbf{H}_l\mathbf{u}_t, \qquad \mathbf{y}_{2t} = \mathbf{A}_r\mathbf{x}(t) + \mathbf{H}_2\mathbf{u}_t \tag{11}$$

where

$$\mathbf{y}_{lt} = \mathbf{S}_{li}^T\mathbf{y}_t, \qquad \mathbf{y}_{2t} = \mathbf{S}_{ld}^T\mathbf{y}_t$$

with

$$\mathbf{H}_1 = \mathbf{S}_{li}^T\mathbf{H}, \qquad \mathbf{H}_2 = \mathbf{S}_{ld}^T\mathbf{H}.$$

Eliminating $\mathbf{x}(t)$ from (11)

$$\mathbf{y}_{2t} = [(\mathbf{H}_2 - \mathbf{A}_r\mathbf{H}_1) \quad \mathbf{A}_r] \begin{bmatrix} \mathbf{u}_t \\ \mathbf{y}_{lt} \end{bmatrix}. \tag{12}$$

The matrix $\mathbf{A}_r$ in (11) and (12) is a $(p \times n)$ matrix containing the rows of $\mathbf{A}_o$ with nonzero nonunity elements, whose locations in $\mathbf{A}_o$ are specified by the selector vector $\mathbf{v}_a$. Equation (12) may be expressed in a more concise form by

$$\mathbf{y}_{2t} = [\mathbf{N}_r \quad \mathbf{A}_r]\mathbf{z}_t \tag{13}$$

where $\mathbf{N}_r = \mathbf{H}_2 - \mathbf{A}_r\mathbf{H}_1$ is a $p \times (\nu+1)m$ matrix and $\mathbf{z}_t$ is an h-dimensional vector containing $\mathbf{u}_t$ and $\mathbf{y}_{1t}$, where $h = (\nu+1)m + n$. Equation (13) is referred to as the *identification identity* since it relates input/output data samples arranged into columns $\mathbf{y}_{2t}$ and $\mathbf{z}_t$ to parameters of the state space representation R_o, i.e., in the matrices $\mathbf{A}_o$, $\mathbf{B}_o$, and $\mathbf{D}_o$.

We now consider the case where only input/output data is available, without a given system model. The process of creating a system model from the data is called system identification. A deterministic D-T system identification will be performed by calculating an observable form state-space model $R_o = \{\mathbf{A}_o, \mathbf{B}_o, \mathbf{C}_o, \mathbf{D}_o\}$ from a set of input and corresponding output data with the restriction that the input signals are "persistently exciting." The technique is based on the identification identity, (13).

In order to determine $\mathbf{N}_r$ and $\mathbf{A}_r$, as well as to select an appropriate set ν of indexes, the following is suggested. Concatenate the vectors $\mathbf{y}_{2t}$ and $\mathbf{z}_t$ corresponding to samples $t = 0, 1, 2, \cdots, q-1$ into $(p \times q)$ and $(h \times q)$ matrices $\mathbf{Y}_2$ and $\mathbf{Z}$, respectively, (where it is assumed that $h < q$ and $q + \nu < N$), yielding

$$\mathbf{Y}_2 = [\mathbf{N}_r | \mathbf{A}_r]\mathbf{Z} \tag{14}$$

where

$$\mathbf{Z} = \begin{bmatrix} \mathbf{U} \\ \hline \mathbf{Y}_1 \end{bmatrix} \begin{matrix} \}(\nu+1)m \\ \\ \}n. \end{matrix}$$

One can quickly conclude that the input sequence used to generate the response is "sufficiently rich" if and only if the matrix $\mathbf{U}$ is full rank, i.e.,

$$\operatorname{rank} \mathbf{U} = (\nu+1)m \tag{15}$$

and that the set of indexes is admissible if $\mathbf{Z}$ is of full (row) rank, i.e., if

$$\operatorname{rank} \mathbf{Z} = h \tag{16}$$

the *condition number* of $\mathbf{Z}$ is relatively large, it might be advisable to try another set of indexes which, through a different set of selector vectors and matrices, could lead to a better conditioned $\mathbf{Z}$. Finally, the solution of (14), containing the parameter information for R_o, is

$$[\mathbf{N}_r | \mathbf{A}_r] = \mathbf{Y}_2\mathbf{Z}^T(\mathbf{Z}\mathbf{Z}^T)^{-1} \tag{17}$$

which reduces to $\mathbf{Y}_2\mathbf{Z}^{-1}$ if the matrix $\mathbf{Z}$ is square. Using the natural structure described above, the POF realization R_o can be constructed from the result of (17). In the next section the technique for system identification is explained.

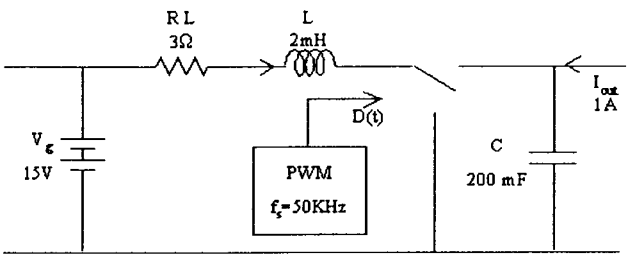

Fig. 2. Boost converter (with PWM control over the switch).

III. A Small-Signal Analysis of Various Converters

As an example of the small-signal analysis of nonlinear dynamic systems under study, an open-loop boost converter, a series resonant converter (SRC), and a forward multiresonant converter (FMRC) are selected. Since the existing state-space averaged model is quite accurate up to the half of the switching frequency in case of the boost converter, the proposed black-box approach can be compared and its effectiveness and accuracy verified.

A. Open-Loop Boost Converter

Fig. 2 illustrates a typical two-state boost converter example. Three input variables and two output variables represent the state of the system dynamics: $\hat{v}_g$ (the variation of input voltage), $\hat{C}_o$ (the variation of input current), and $\hat{d}$ (the variation of duty cycle), $\hat{C}_l$ (the variation of output inductor current), $\hat{v}_c$ (the variation of output capacitor voltage). This converter was designed to operate at a nominal duty ratio of 0.6 with an efficiency of 70.5%. The exact discrete state-space equation including all the nonlinearities is used for the time-domain simulation.

As described in detail [7], the procedure is summarized as follows

Step 1: A small range of elaborate input perturbations around a nominal equilibrium point is injected at the inputs of the boost converter, such as, $\hat{v}_g$, $\hat{C}_o$, and $\hat{d}$, and then the corresponding output responses are measured in physical unit. Generally, small-signal analysis of an unknown system, unlike the above boost converter, must be done using a circuit simulation tool such as PSpice or the measurement data from the hardware directly. Therefore, extracting information from data is not a straightforward task. In addition to the decisions required for model structure selection and generalization, the collected data need to be handled carefully for the proposed identification process. The levels in these raw inputs and outputs should be matched in a consistent way. The mean levels must be subtracted from the input and output sequences before the estimation. The best way is to match the mean levels corresponding to a system equilibrium.

Step 2: The second step is to determine a nominal range of the system order with the restriction that the input signals are "persistently exciting." From the assumption that the order of the system is unknown, to determine the system order from raw data, a rank test is done. However, due to the nonlinearity of the system with added noise, a rank test may not be reliable.

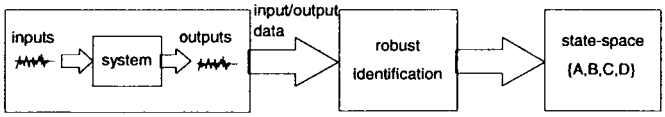

Fig. 3. Small-signal analysis process.

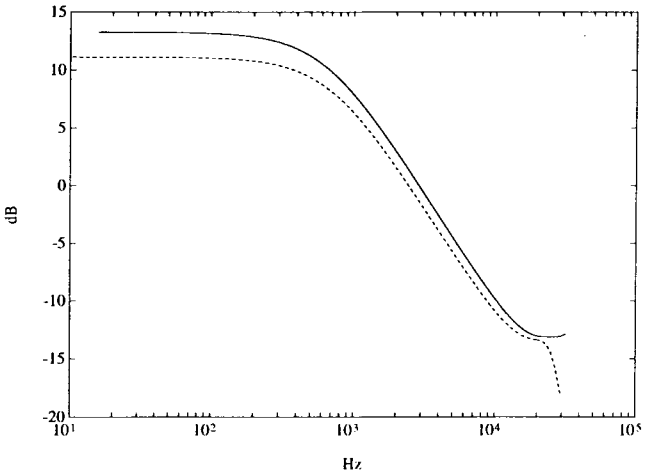

Fig. 4. Magnitude: identified (solid), state-space averaging (dotted).

Step 3: The third step is to construct an ARMA model with inputs representing both the present inputs and delayed versions of the inputs and outputs to capture the dynamics of the systems. The method determines an equilibrium point to identify a linearized system about this equilibrium point. It is a classical method of multivariable system identification which utilizes the possible structures of the system in order to achieve a model that optimally generalizes over the available input/output data.

Step 4: The final step, a deterministic D-T system identification, is performed by calculating an observable form state-space model $\boldsymbol{R_o} = \{\boldsymbol{A}, \boldsymbol{B}, \boldsymbol{C}, \boldsymbol{D}\}$ from the identified ARMA model. The small-signal modeling process is shown in Fig. 3.

Using the proposed identification technique, a small-signal analysis of the boost converter is developed as the following ARMA model:

$$\boldsymbol{y}(k) = \sum_{i=1}^{n} a_{k-i}\boldsymbol{y}(k-i) + \sum_{i=0}^{n} b_{k-i}\boldsymbol{u}(k-i) \qquad (18)$$

where $y_1 = \hat{\mathbb{C}}_l$, $y_2 = \hat{v}_c$, $u_1 = \hat{v}_g$, $u_2 = \hat{\mathbb{C}}_o$, and $u_3 = \hat{d}$. From (18) it is noted that delayed inputs and outputs contribute to the "predicted" output. Since the boost converter is second order, the ARMA model of the linearized system is expected to have $u_1(k)$, $u_1(k-1)$, $u_2(k)$, $u_2(k-1)$, $u_3(k)$, $u_3(k-1)$, $y_1(k-1)$, and $y_2(k-1)$ terms. For reference, the eigenvalues of the C-T equivalent model of (18) are $\{-1166.6, -347.5\}$ comparing with those of state-space averaged model of the exact system equation, $\{-1153.1, -346.9\}$. When duty cycle $\hat{d}$ is modulated, the magnitude and the phase of the control-to-output transfer function of the identified model are compared against the state-space averaged model of the system in Figs. 4 and 5, respectively. The obtained small-signal model is accurate up to half of the switching frequency, i.e., 25 kHz (Nyquist frequency).

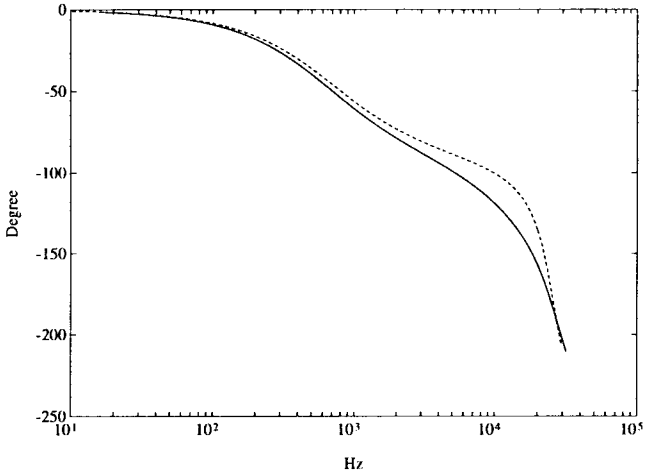

Fig. 5. Phase: identified (solid), state-space averaging (dotted).

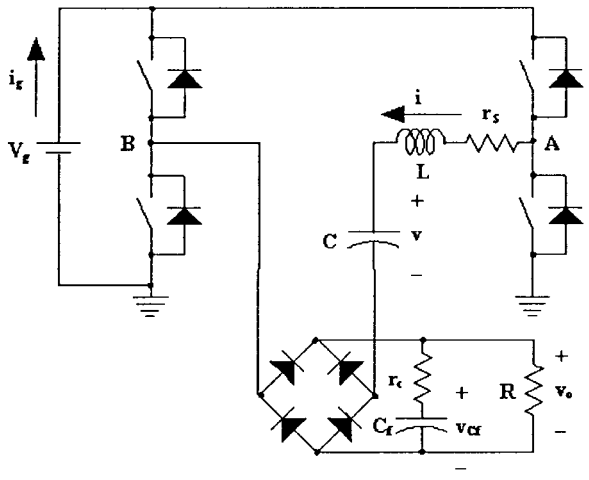

Fig. 6. Series resonant converter.

B. Series-Resonant Converter (SRC)

The small-signal analysis for an SRC based on the proposed identification technique is discussed in this section. Among several approaches for modeling an SRC, the well-known state-space averaging technique does not show promising results in modeling for resonant converters, where the energy of the system is carried mainly by the switching frequency harmonics (not by the low-frequency components as in the case of PWM converters). Since the dynamics are often determined by the interaction between the switching frequency and the natural frequency of the resonant converter, state-space averaging eliminates the useful information of this interaction between both frequencies. Therefore, the previous identification procedure was applied to the input/output data streams of nonlinear system equations of an SRC [7]. The identified model was compared with the analytical result to verify the correctness of the procedure. The circuit diagram of the SRC is shown in Fig. 6. The circuit parameters and the

operating point are the following:

$$\begin{aligned} L &= 197\ \mu\text{H} & C &= 51\ \text{nF} \\ C_f &= 3\ \mu\text{F} & r_c &= 0 \\ F_o &= 50.2\ \text{kHz} & Z_o &= 62.1\ \Omega & r_s &= 0. \\ V_g &= 62.15\ \text{V} & D &= 0.95 \\ F_s/F_o &= 0.85, & Q_s &= Z_o/R = 2.5 \end{aligned}$$

The active switch network generates a quasi-square voltage v_{AB} applied to the resonant tank. By assuming the continuous mode of the inductor current (tank current i), the SRC can be modeled as in the following nonlinear state equations:

$$\begin{aligned} L\frac{di}{dt} + v + \text{sgn}(i)v_o &= v_{AB} \\ C\frac{dv}{dt} &= i \\ C_f\, d\frac{v_o}{dt} + \frac{v_o}{R} &= |i|. \end{aligned} \tag{19}$$

There are three input variables: $\hat{v}_g$ (the variation of input voltage), $\hat{\subset}_o$ (the variation of output current), and $\uparrow$ (the variation of switching frequency), and three output variables: $\hat{\subset}_g$ (the averaged input current), $\hat{v}_{Cf}$ (the capacitor C_f output voltage), and $\hat{v}_o$ (the output voltage) of the power stage. In this configuration, the output voltage is regulated by modulating the switching frequency $\uparrow$. The resulting small-signal model of the SRC is given below as a state-space representation form $\boldsymbol{R_o} = \{\boldsymbol{A}, \boldsymbol{B}, \boldsymbol{C}, \boldsymbol{D}\}$

$$\begin{bmatrix} \mathbf{A} \\ \hline \mathbf{C} \end{bmatrix} = \left[\begin{array}{rrr} 0.3367 & -0.0094 & -0.0011 \\ 23.5832 & 0.7523 & 0.3472 \\ 1.4497 & -0.0345 & 0.9702 \\ \hline 1 & 0 & 0 \\ 0 & 1 & 0 \\ 0 & 0 & 1 \end{array}\right]$$

$$\begin{bmatrix} \mathbf{B} \\ \hline \mathbf{D} \end{bmatrix} = \left[\begin{array}{rrr} 0.4396 & 0.0014 & 0.0110 \\ -24.2318 & 0.4943 & -0.2752 \\ 2.6661 & 0.0113 & -0.6898 \\ \hline 0.3282 & 0.0083 & 0.0074 \\ -79.4499 & 0.1109 & -0.3381 \\ 0.6759 & 0.0108 & -0.4351 \end{array}\right]. \tag{20}$$

Figs. 7 and 8 show the control-to-output transfer function of the SRC compared against the measured data. The numerical results are in good agreement with the measured data.

C. Forward Multiresonant Converter (FMRC)

The whole circuit has six energy storage elements and the resonant tank formed by L, C_s, and C_d is the third order. The magnetizing inductance is denoted by L_m. The FMRC is controlled by varying the turn-on time of the active switch (S), and the turn-off time is fixed. The advantage of this topology

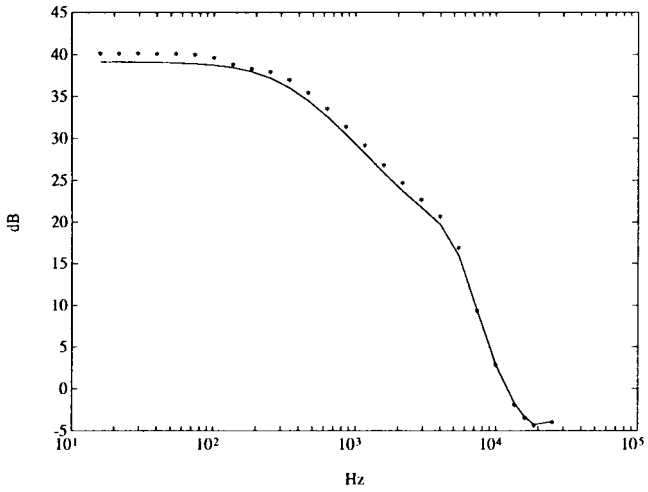

Fig. 7. Magnitude: identified (solid), measured (*).

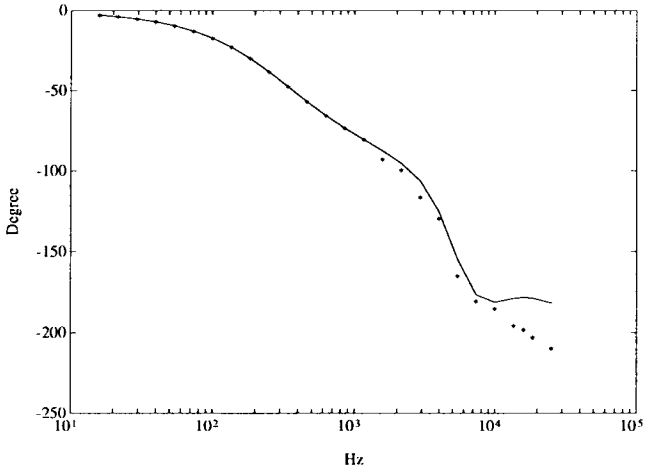

Fig. 8. Phase: identified (solid), measured (*).

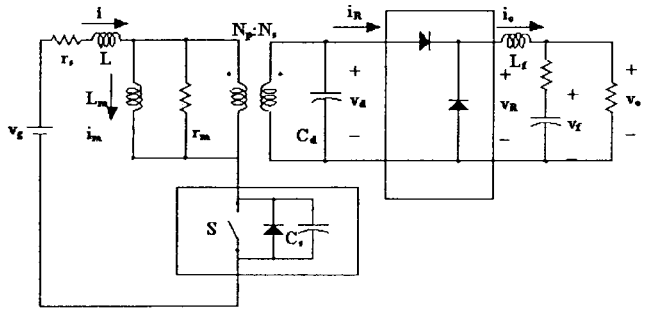

Fig. 9. Forward multiresonant converter.

is that it absorbs the major circuit parasitics such as the output capacitance of the switching devices, the junction capacitance of the rectifier diodes, and the leakage inductance of the transformer. Furthermore, all of the semiconductor devices can be operated under zero voltage switching condition with proper design. Since several operating modes exist for this circuit with respect to different loads and switching frequencies, therefore, it is not feasible to obtain dc characteristics analytically. Especially, there are two resonant frequencies for the FMRC, corresponding to the turn-on period and the turn-off period,

respectively. This makes the FMRC a more difficult circuit than the other resonant converters for modeling. The FMRC are built as the following parameters:

$$\begin{aligned} L &= 45\ \mu\text{H} & C_s &= 48.2\ \text{nF} \\ L_m &= 139\ \mu\text{H} & C_d &= 661\ \text{nF} \\ L_f &= 82\ \mu\text{H} & C_f &= 34\ \mu\text{F} \\ n &= 2 & r_s &= 0.63\ \Omega \\ r_c &= 206\ \text{m}\Omega & r_m &= 7.3\ \text{k}\Omega \\ F_o &= 108.1\ \text{kHz} & Z_o &= 30.6\ \Omega. \end{aligned}$$

The nonlinear state equations of the FMRC are the following:

$$\begin{aligned} L\frac{di}{dt} + ir_s + v_s + \frac{v_d}{n} &= V_g \\ C_s\frac{dv_s}{dt} &= S_a i \\ L_m\frac{di_m}{dt} &= \frac{v_d}{n} \\ C_d\frac{dv_d}{dt} &= n\left(i - i_m - \frac{nv_d}{r_m}\right) i_R \\ L_f\frac{di_o}{dt} &= v_r - v_o \\ C_f\, d\frac{v_f}{dt} &= i_o - \frac{v_o}{R} \end{aligned} \tag{21}$$

where S_a represents the switching action of the MOSFET

$S_a = 0$ MOSFET or its body diode ON

$S_a = 1$ otherwise.

The parasitics related with losses are defined by

r_s conduction loss of the tank;

r_m core loss of the transformer;

r_c ESR of the output capacitor.

With the above large-signal nonlinear model available, time domain simulation is done with PSpice in the Appendix. There are three input variables, $\hat{v}_g$, $\hat{C}_o$, $\hat{d}$, and six output variables, $\hat{C}_l$, $\hat{C}_{lm}$, $\hat{C}_{lf}$, $\hat{v}_{cs}$, $\hat{v}_{cd}$, and $\hat{v}_o$ of the power stage. To verify the results of the analysis, an FMRC was built with the same component values as shown above. Figs. 10 and 11 show the control-to-output transfer function of the small-signal model of the FMRC compared with the measured data. The identified results of both gain and phase are close to the measured data except near the one-half of the switching frequency, which shows the difficulty of this problem.

The identified small-signal model of the FMRC is given below as a state-space representation form $\boldsymbol{R_o} = \{\boldsymbol{A}, \boldsymbol{B}, \boldsymbol{C}, \boldsymbol{D}\}$ as shown, at the bottom of the page, in (22).

D. Full-Bridge Zero-Voltage-Switched (FB-ZVS) PWM Converter

In contrary to the conventional PWM converters, the circuit parasitics such as the output capacitances of the switching devices and the leakage inductance of the high-frequency transformer have beneficial effects on the converter perfor-

$$\begin{bmatrix} \mathbf{A} \\ \hline \mathbf{C} \end{bmatrix} = \left[\begin{array}{cccccc} -12.317 & 0.4516 & 0.5953 & 293.372 & 0.0367 & -0.394 \\ 0.63 & 0.5219 & -0.3427 & -412.149 & -0.0271 & 0.187 \\ -0.865 & -0.8106 & 1.2722 & 933.758 & -0.0466 & 0.357 \\ -0.002 & 0.0005 & 0.0005 & 2.718 & 0.0000 & -0.000 \\ -15.717 & -2.9882 & -2.2787 & 1370.856 & -0.0942 & -3.133 \\ 0.017 & -0.0786 & 0.3058 & -2.964 & -0.0043 & 0.933 \\ \hline 1 & 0 & 0 & 0 & 0 & 0 \\ 0 & 1 & 0 & 0 & 0 & 0 \\ 0 & 0 & 1 & 0 & 0 & 0 \\ 0 & 0 & 0 & 1 & 0 & 0 \\ 0 & 0 & 0 & 0 & 1 & 0 \\ 0 & 0 & 0 & 0 & 0 & 1 \end{array}\right]$$

$$\begin{bmatrix} \mathbf{B} \\ \hline \mathbf{D} \end{bmatrix} = \left[\begin{array}{ccc} -0.0651 & 0.0258 & -9.7244 \\ 0.0009 & -0.0058 & -1.0201 \\ 0.0691 & -0.0026 & -1.3769 \\ -0.0001 & 0.0000 & -0.0094 \\ -0.0101 & 0.6498 & -73.8649 \\ 0.0214 & 0.1051 & 1.0132 \\ \hline -0.0973 & -0.1201 & -3.4953 \\ 0.0488 & 0.0234 & 7.9658 \\ 0.0575 & 0.0083 & 4.8434 \\ -0.0001 & -0.0001 & -150.0035 \\ -0.4763 & -0.5441 & 6.3498 \\ 0.0046 & 0.1186 & 0.2315 \end{array}\right]. \tag{22}$$

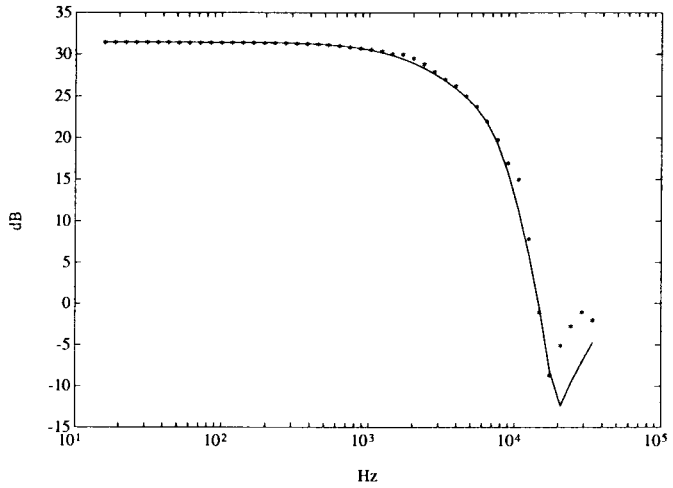

Fig. 10. Magnitude: identified (solid), measured (*).

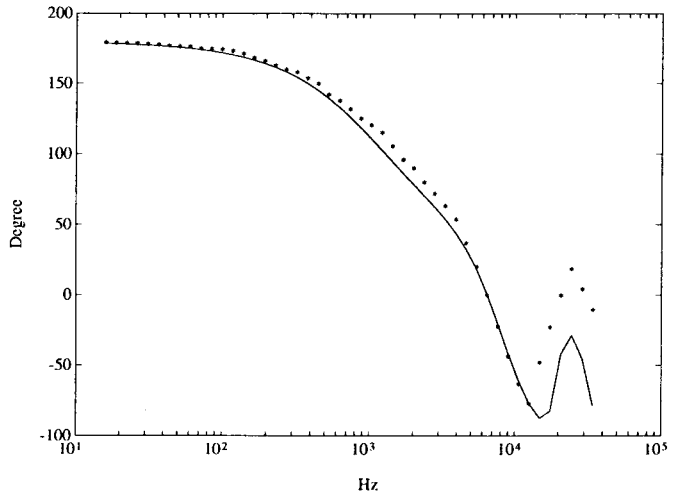

Fig. 11. Phase: identified (solid), measured (*).

mance in ZVS topology. With phase-shift control, transformer leakage inductance and MOSFET's junction capacitance can be utilized to achieve zero-voltage resonant switching, which enables high-frequency operation for improved efficiency and reduced volume and weight. Considering the recently increased attention to this ZVS topology, the small-signal analysis of this type of converter is necessary, but only a few researchers have focused on this problem [3], [8]. This ZVS PWM converter topology seems to be very close to the conventional PWM converter topology, but its small-signal properties are found to be significantly different from those of the PWM converter, and its small-signal analysis is hard to be achieved by state-space averaging because of the presence of a large leakage inductance and the phase-shift control.

In this section, the small-signal analysis of the ZVS PWM converter is achieved by the proposed identification technique using the help of circuit simulation program such as PSpice.

The ZVS PWM converter constructed in Fig. 12 has the following circuit parameter values [8]:

$$\text{Input voltage, } V_{\text{in}} = 600 \text{ V}$$
$$\text{Output voltage, } V_{\text{out}} = 360 \text{ V}$$

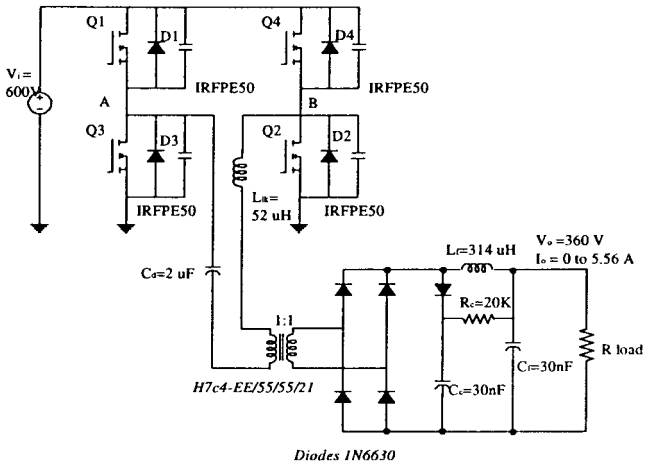

Fig. 12. The FB-ZVS PWM converter.

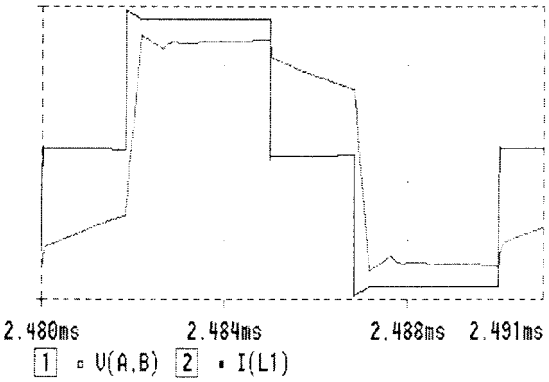

Fig. 13. Simulated waveforms.

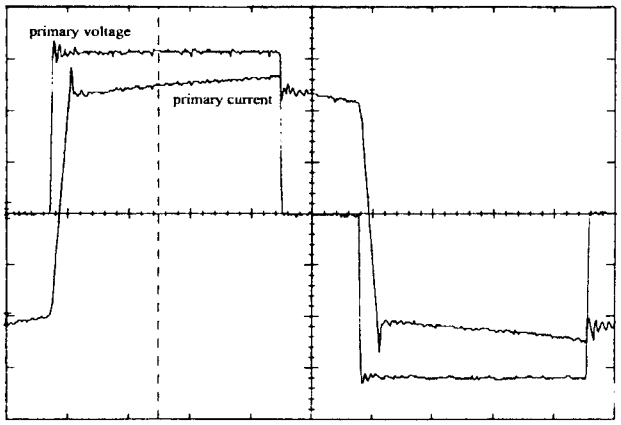

Fig. 14. Experimental waveforms.

$$\text{Output capacity, } P_{\text{out}} = 2 \text{ kW}$$
$$\text{Transformer turns ratio, } n = 1$$
$$\text{Transformer leakage inductance, } L_{lk} = 52\ \mu\text{H}$$
$$\text{Output filter inductor, } L_f = 314\ \mu\text{H}$$
$$\text{Output filter capacitor, } C = 5\ \mu\text{F}$$
$$\text{DC blocking capacitor, } C_d = 2\ \mu\text{F}.$$

The results of both simulated and also experimental waveforms showing the ZVS effects are given in Figs. 13 and 14.

Figs. 15 and 16 show the control-to-output transfer function of the FB-ZVS-PWM converter compared with the measure-

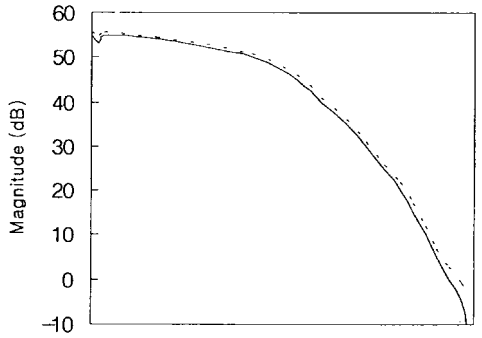

Fig. 15. Magnitude: identified (solid), measured (dashed).

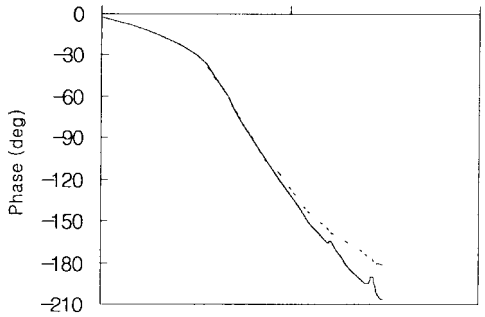

Fig. 16. Phase: identified (solid), measured (dashed).

ment data. The numerical results of both gain and phase measurements are in good agreement with predictions.

IV. Conclusions

As a unified black-box modeling approach of highly nonlinear power electronics systems, a novel identification technique is proposed for modeling conventional switching converters, resonant converters, and full-bridge ZVS converterts. In order to get not only physical insight of system but also to have a convenient linearized model of the given system at the specific operating point, a small-signal modeling method is introduced using PSpice and MATLAB along with the classical linear identification method. A boost converter, an SRC, an FMRC, and a ZVS PWM converter are taken as examples to demonstrate the proposed algorithm and the result looks very promising even though the key factor is how to persistently excite the system for showing all kinds of characteristics to be identified.

Appendix

==> Forward Multiresonant Converter

```
* Measured Outputs:
*- - - - - - - - - - - - - - - - - -
* 1) i(L)
* 2) i(Lm)
* 3) i(Lf)
* 4) VCf              ===> node (4)
* 5) VCd              ===> node (20)
  EVcd    (20,0) (5,6)    1
  Rvcd    (20,0)          1
* 6) Vo               ===> node (21)
  EVo     (21,0) (9,6)    1
  RVo     (21,0)          1

*- - - - - - - CIRCUIT DESCRIPTION.....

* ==> Vg is an input .....................................................
  Vg              (1,vn)  35.2
  Evn     (vn,0) (vn0,0) 1
  Rvn             (vn0,0) 1
* This is a VCVS: change the gain to control the size of
perturbation

*Vn (vn0,0) PWL (0 1 11.3u 1 11.301u -.4 22.6u -.4 22.601u
.4 33.9u .4 33.901u -1 45.2u -1 45.201u 0 56.5 0)
*Vn (vn0,0) PWL (0 2 11.3u 2 11.301u -.2 22.6u -.2 22.601u
.2 33.9u .2 33.901u -2 45.2u -2 45.201u 0 56.5 0)
*Vn (vn0,0) PWL (0 -.3 11.3u -.3 11.301u -.9 22.6u -.9
22.601u .3 33.9u .3 33.901u .9 45.2u .9 45.201u 0 56.5 0)
*Vn (vn0,0) PWL (0 -.7 11.3u -.7 11.301u -1.1 22.6u -1.1
22.601u .7 33.9u .7 33.901u 1.1 45.2u 1.1 45.201u 0 56.5 0)
Vn (vn0,0) PWL (0 -.5 11.3u -.5 11.301u -.1 22.6u -.1
22.601u .5 33.9u .5 33.901u .1 45.2u .1 45.201u 0 56.5 0)

* ==> In is an input .....................................................
  Gn      (6,8)  (30,0)  0.4
  Rn             (30,0)  1
* This is a VCCS: Change the gain to control the size of
perturbation

*Vi (30,0) PWL (0 1 11.3u 1 11.301u -.4 22.6u -.4 22.601u .4
33.9u .4 33.901u -1 45.2u -1 45.201u 0 56.5 0)
*Vi (30,0) PWL (0 2 11.3u 2 11.301u -.2 22.6u -.2 22.601u .2
33.9u .2 33.901u -2 45.2u -2 45.201u 0 56.5 0)
*Vi (30,0) PWL (0 -.3 11.3u -.3 11.301u -.9 22.6u -.9 22.601u
.3 33.9u .3 33.901u .9 45.2u .9 45.201u 0 56.5 0)
Vi (30,0) PWL (0 -.7 11.3u -.7 11.301u -1.1 22.6u -1.1
22.601u .7 33.9u .7 33.901u 1.1 45.2u 1.1 45.201u 0 56.5 0)
*Vi (30,0) PWL (0 -.5 11.3u -.5 11.301u -.1 22.6u -.1 22.601u
.5 33.9u .5 33.901u .1 45.2u .1 45.201u 0 56.5 0)

  Rs              (1,2)   0.63
  L               (2,3)   45u      ic = -4.010 238 2
  Lm              (3,4)   139u     ic = 1.035 218 7
  Rm              (3,4)   7.3K

  Cs              (4,0)   48.2n    ic = 9.721 489 9
  Diode           (0,4)            DIODE
  Sd      (4,0)   (d,0)            SWITCH

* ..... Duty cycle control .....

  Ed      (sense,0) poly(2) (ramp,0) (40,0) 0 -1000 1000
  Rdz     (sense,d)       10
  Dzener  (0 ,d) ZENER

* Ramp voltage 0->1V 11.3 usec period
  Vramp   (ramp,0) PULSE (0 1 0 11.298u 1n 1n 11.3u)
  Rramp   (ramp,0) 1

* Nominal duty cycle
  Vd      (40,vdn)    0.619 469
  Edn     (vdn ,0 ) (dn0,0) 0.1
```

```
  Rcntr (40,0)     1
  Rd    (dn0,0)    1
* This is a VCVS: change the gain to control the size of
perturbation

*Vdn (dn0,0) PWL (0 1 11.3u 1 11.301u -.4 22.6u -.4 22.601u
.4 33.9u .4 33.901u -1 45.2u -1 45.201u 0 56.5 0)
*Vdn (dn0,0) PWL (0 2 11.3u 2 11.301u -.2 22.6u -.2 22.601u
.2 33.9u .2 33.901u -2 45.2u -2 45.201u 0 56.5 0)
Vdn (dn0,0) PWL (0 -.3 11.3u -.3 11.301u -.9 22.6u -.9
22.601u .3 33.9u .3 33.901u .9 45.2u .9 45.201u 0 56.5 0)
*Vdn (dn0,0) PWL (0 -.7 11.3u -.7 11.301u -1.1 22.6u -1.1
22.601u .7 33.9u .7 33.901u 1.1 45.2u 1.1 45.201u 0 56.5 0)
*Vdn (dn0,0 ) PWL (0 -.5 11.3u -.5 11.301u -.1 22.6u -.1
22.601u .5 33.9u .5 33.901u .1 45.2u .1 45.201u 0 56.5 0)



* ..... Ideal Tranformer.....
  RXFORM (4 , 6) 1MEG
  FXFORM (3 , 4) VXFORM 0.5
  VXFORM (5x, 5) 0
  EXFORM (5x, 6) (3 , 4) 0.5
* .....
  Cd    (5,6)     661n      ic = -5.228 753 1
  D1    (5,7)     DIODE
  D2    (6,7)     DIODE
  Lf    (7,8)     82u       ic = 3.243 697 2
  Rc    (8,9)     206m
  Cf    (9,6)     34u       ic = 8.230 114 9
  Rload     (8,6)     2.8152



*+++++ SIMULATION COMMANDS +++++++

.OPTION PIVTOL=1E-99 ITL5=0 NUMDGT=8
NOECHO NOMOD
.WIDTH OUT = 132
.MODEL SWITCH VSWITCH (Ron = 1m Roff = 1Meg Von
= 10 Voff = 0.5)
.MODEL ZENER D (BV = 10)
.MODEL DIODE D ()
.tran 11.3u 56.5u 0 0.2u UIC
.print tran v(1) v(30) v(40) i(L) i(Lm) i(Lf) v(4) v(20)
v(21)
* <- - - Inputs - - -> <- - - - - - - - - - - - -
Outputs - - - - - - - - - - - - ->
* Vg Io d            Vcs Vcd Vo
.probe
.end



* Schematics Netlist*
R_Rs     1 2 0.63
L_L 2 3 45uH IC=-4.010 238 2
L_Lm     3 4 139uH IC=1.035 218 7
R_rm     4 3 7.3k
C_Cd     5 6 661n IC=-5.228 753 1
L_Lf     7 8 82uH IC=3.243 697 2
R_Rload     6 8 2.8
R_Rc     9 8 206m
C_Cf     9 6 34u IC=8.230 114 9
D_D6     5 7 Dbreak
D_D7     6 7 Dbreak
R_RXFORM         4 6 1Meg
V_Vg     1 $N_0001 DC 35.2V
E_Evn    $N_0001 0 $N_0002 0 1
V_Vn     $N_0002 0 PWL FILE
"c:\user\paper\spice\fmrc\vn.dat"
R_Rvn    $N_0002 0 1
G_G1     6 8 30 0 0.4
V_V9     30 0 PWL FILE
"c:\user\paper\spice\fmrc\current.dat"
R_Rn     30 0 1
S_S1     4 0 d 0 Sbreak-X
RS_S1    d 0 1G
D_D8     0 4 Dbreak
C_Cs     4 0 48.2n IC=9.721 489 9
E_DIFF1  $N_0003 0 VALUE {V($N_0005,$N_0004)}
E_ABM11  $N_0005 0 VALUE { (V(40) * 1000) }
E_ABM12  $N_0004 0 VALUE { (V(ramp) * 1000) }
E_E2     sense 0 $N_0003 0 1
R_Rdz    sense d 10
R_Rd     $N_0006 0 1
V_Vdn    $N_0006 0 PWL FILE
"c:\user\paper\spice\fmrc\t2.dat"
E_Edn    $N_0007 0 $N_0006 0 0.1
V_Vd     40 $N_0007 DC 0.619 469
R_Rramp  ramp 0 1
V_Vramp  ramp 0
+PULSE 0 1 0 11.298u 1n 1n 11.3u
R_Rcntr  40 0 1
F_F1     3 4 VF_F1 0.5
VF_F1    5x 5 0V
E_E5     5x 6 3 4 0.5
D_Dzener 0 d DbreakZ
```

REFERENCES

[1] V. Vorperian, "Simplified analysis of PWM converters using the model of the PWM switch: Parts I and II," *IEEE Trans. AES*, vol. 26, no. 3, pp. 490–505, 1990.

[2] V. Vorperian and S. Cuk, "Small-signal analysis of resonant converters," in *Proc. IEEE PESC*, 1983, pp. 269–282.

[3] V. Vlatkovic, J. A. Sabate, R. B. Ridley, F. C. Lee, and B. H. Cho, "Small-signal analysis of the zero-voltage switched full-bridge PWM converter," in *High Frequency Power Conversion Conf.*, May 1990, pp. 262–272.

[4] D. G. Luenberger, "Canonical forms for linear multivariable systems," *IEEE Trans. Automat. Contr.*, vol. AC-12, pp. 290–293, 1967.

[5] T. Kailath, *Linear Systems*. Englewood Cliffs, NJ: Prentice Hall, Inc., 1980.

[6] S. Bingulac and H. F. VanLandingham, *Algorithms for Computer-Aided Design of Multivariable Control Systems*. New York, NY: Marcel Dekker, 1993.

[7] J. Y. Choi, "Nonlinear system identification and control using neural networks," Ph.D. dissertation, VPISU, Blacksburg, VA, 1994.

[8] J. A. Sabate, V. Vlatkovic, R. B. Ridley, F. C. Lee, and B. H. Cho, "Design considerations for high-voltage high-power full-bridge zero-voltage-switched PWM converter," in *Proc. IEEE APEC*, 1990, pp. 275–284.

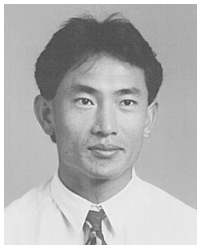

Ju-Yeop Choi (M'97) received the B.S. degree from Seoul National University, Seoul, Korea in 1983, the M.S. degree from University of Texas at Arlington, TX in 1990, and the Ph.D. degree from Virginia Tech in 1994, all in electrical engineering. Since 1995, he has been with the Intelligent System Control Research Center of Korea Institute of Science and Technology. His research interests are in modeling and control of power electronics and industrial processes such as steam boiler system using neuro-fuzzy algorithm.

Bo H. Cho (M'89–SM'95) received the B.S. and M.S. degrees from California Institute of Technology and the Ph.D. degree from Virginia Polytechnic Institute and State University, all in electrical engineering.

From 1980 to 1982, he worked as a Member of Technical Staff of Power Conversion Electronics Department, TRW Defense and Space System Group. From 1982 to 1995, he was a faculty member in the Department of Electrical Engineering, VPI&SU, Blacksburg VA. In 1995, he joined the Electrical Engineering Department of Seoul National University, Seoul, Korea, where he is currently an Associate Professor.

His main research interests include, modeling, analysis and control of power electronics circuits and systems, high frequency power conversion, spacecraft power processing systems, and distributed power systems.

Dr. Cho was a recipient of the 1989 NSF Presidential Young Investigator Award.

Hugh F. VanLandingham (S'56–M'66–SM'80) is a professor of electrical and computer engineering. Since he received the Ph.D. degree at Cornell University in 1967, he has been with Virginia Tech in Blacksburg, VA. He is the author or co-author of three textbooks and more than 60 published technical papers. His interests are in control of industrial processes, including applications of neural networks and fuzzy logic.

Hyung-soo Mok (S'87–M'97) received the B.S., M.S., and Ph.D. degrees from Seoul National University, Seoul, Korea, in 1986, 1988, and 1992, respectively. He was with the Department of Control and Instrumentation Engineering at the Seoul National Polytechnic University as an Associate Professor from 1993 to 1997. Since 1997, he has been with the Department of Electrical Engineering at Kon-Kuk University as an Associate Professor. His present research interests are in power electronics, machine control and simulation techniques using PSpice, MATLAB, and SABER.

Joong-Ho Song (M'97) received the B.S. and M.S. degrees in electrical engineering from Seoul National University, and the Ph.D. degree in electrical engineering from KAIST in 1980, 1982, and 1993, respectively. From 1982 to 1985, he was employed by E-Hwa Electrical Co. Since 1985, he has been with the Intelligent System Control Research Center, KIST. He was a Visiting Scholar in the WEMPEC, University of Wisconsin, Madison in 1995–1996. His primary areas of interest are in switching converter technology, electric machine drives, and servo control technology.